Journal of Applied Polymer Science

Analyses of Structurally Modified Quasi-Solid-State Electrolytes Using Electrochemical Impedance Spectroscopy for Dye-Sensitized Solar Cells

Seok-Jun Seo,[1,2,3] Andreas Hinsch,[3] Welmoed Veurman,[3] Henning Brandt,[3] Moon-Sung Kang,[4] Sung-Hee Shin,[1] Seung-Hyeon Moon[1,2]

[1]Membrane and Electrochemistry Lab., School of Environmental Science and Engineering, Gwangju Institute of Science and Technology (GIST), 123 Cheomdan-gwagiro, Buk-gu, Gwangju 500-712, Republic of Korea

[2]Energy storage Lab., Research Institute for Solar and Sustainable Energies (RISE), Gwangju Institute of Science and Technology (GIST), 123 Cheomdan-gwagiro, Buk-gu, Gwangju 500-712, Republic of Korea

[3]Fraunhofer Institute for Solar Energy Systems (ISE), Heidenhofstrasse 2, Freiburg 79110, Germany

[4]Department of Environmental Engineering, College of Engineering, Sangmyung University, Cheonan, Chungnam Province 330-720, Republic of Korea

Correspondence to: S.-H. Moon (E-mail: shmoon@gist.ac.kr)

ABSTRACT: Electrochemical properties of structurally modified quasi-solid-state electrolytes were examined using porous substrates (PSs). The PS was prepared into two categories by a phase inversion method with a brominated poly(phenylene oxide) (BPPO): the sponge and finger types. Effects of the humidification and cosolvent compositions on the morphology of the PS were analyzed by scanning electron microscopy. In all cases of the PSs, a higher V_{OC} was observed of about 0.1 V than that of a liquid electrolyte owing to a suppressed back electron charge transfer. In addition, the PS prepared by the polymer solution of 1 : 4 : 1 (BPPO : *N*-methyl-2-pyrrolidone : butyl alcohol) with the humidification process showed better photovoltaic properties in terms of the current density and conversion efficiency owing to the appropriate combinations of pore size, tortuosity, and interconnectivity. Effects of the pore structures were intensively examined using electrochemical impedance spectroscopy. The impedance results revealed that large pores at the surface layers are advantageous for a lower R_S and R_{TiO2}. Meanwhile, the straight inner structure is beneficial for the facile I^-/I_3^- diffusion, thus lowering R_{Pt}. © 2013 Wiley Periodicals, Inc. J. Appl. Polym. Sci. **2014**, *131*, 39739.

KEYWORDS: electrochemistry; properties and characterization; morphology; optical and photovoltaic applications; porous materials

Received 26 February 2013; accepted 6 July 2013
DOI: 10.1002/app.39739

INTRODUCTION

Dye-sensitized solar cells (DSSCs) have been attracted considerable interests as an alternative to conventional silicon solar cells since the report by Grätzel and O'Regan.[1] DSSCs are regarded as one of the environmentally benign energy sources owing to advantages such as the simple fabrication process, low production cost, and commercially realistic energy-conversion efficiency up to 12%.[2–4] However, there are some critical obstacles using liquid electrolytes in terms of a perfect sealing to prevent leakage, minimizing the volatility of electrolytes without sacrifice of conductivity, and ensuring safety requirements of low flammability and toxicity. Recently, to overcome the leakage problem, gel-type electrolytes and solid-state electrolytes have been widely investigated.[5–8] In addition, quasi-solid-state electrolytes have been studied and obtained comparably high efficiency to the liquid electrolyte as well as good long-term stability similarly to the gel and solid-state electrolytes.[9–15]

There are two preparation types of porous substrates (PSs) utilized for quasi-solid-state electrolytes: (1) electrospinning method and (2) phase inversion method. High-performance quasi-solid-state electrolytes have also been prepared using the electrospun nanofiber mats. Priya et al.[9] prepared electrospun nanofiber mat with poly(vinylidene fluoride-*co*-hexafluoropropylene) (PVdF-HFP). By employing the nanofiber mat, the DSSC with the quasi-solid-state electrolyte showed higher V_{OC} with similar J_{SC} to the liquid electrolyte. The physical contact of Lewis basic polymers to the trap sites in the TiO_2 electrode also seems to lower the recombination rates, showing higher V_{OC} values. Significance of the pore size, volume ratio, and three-dimensional interconnectivity of PSs was discussed by Kim

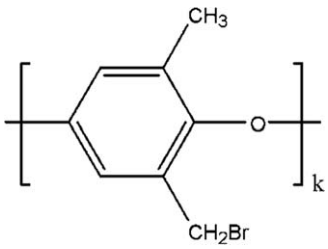

Figure 1. A polymer structure of BPPO.

et al.[10] Blending of PVdF–HFP and polystyrene with blending ratio of 3 : 1 derived higher V_{OC} and fill factor (FF).[11] Furthermore, Lewis basicity of BPPO polymer was compared to the PVdF in the form of electrospun nanofiber mats for quasi-solid-state electrolytes.[12]

Kim et al.[13] prepared a PS using the phase inversion method with a copolymer of acrylonitrile and methyl methacrylate. The PS was immersed in a liquid electrolyte, exhibiting a transparent gel polymer electrolyte and higher V_{OC} than the liquid electrolyte. Zhang et al. prepared PSs of PVdF–HFP to examine the effects of TiO_2 nanoparticles.[14] The PS with 30 wt % TiO_2 particles has fine and uniform pore sizes, which are advantageous for a higher conductivity of the quasi-solid-state electrolyte. *In situ* ultra-thin polymer membrane was also directly introduced onto the TiO_2 layer by a phase inversion method.[15]

However, the effects of morphological changes of PSs for quasi-solid-state electrolytes have yet been systematically investigated in DSSC applications. In this study, surface layers and inner structures of PSs were modified by controlling the solvent compositions and humidifying conditions. Effects of the morphological changes were examined by scanning electron microscopy (SEM), whereas the photovoltaic properties were analyzed by *J–V* curves and electrochemical impedance spectroscopy (EIS).

EXPERIMENTAL

Preparation of Porous Substrates by a Phase Inversion Method

Two types of polymer solutions were prepared; dissolving (i) 2 g of brominated poly(phenylene oxide) (BPPO, $M_w = 70{,}000$) in 10 mL of *N*-methyl-2-pyrrolidone (NMP, Aldrich) (ratio, 1 : 5 : 0) and (ii) 2 g of BPPO in 8 mL of NMP and 2 mL of butyl alcohol (BuOH, Aldrich) (ratio, 1 : 4 : 1), respectively.[16] The polymer structure of the BPPO is shown in Figure 1. Each solution was cast on a glass plate, and then the plate was promptly soaked in deionized water; the porous substrate was obtained without humidification (PS-WOH). To obtain a porous substrate with humidification, the cast polymer on the glass plate was stored in a humidifying container saturated with water vapor in a nitrogen atmospheric condition at 80°C for 10 min, and then the plate was also soaked in deionized water (PS-H). Finally, the porous substrates were dried in an oven at 50°C for more than 3 days.

Fabrication of Quasi-Solid-State DSSCs

To prepare electrodes, a fluorine-doped tin oxide (FTO) conducting glass (8 Ω/sq, Solaronix) was consecutively cleaned with deionized water, detergent, ethanol, and acetone. A photo-anode was prepared by casting a TiO_2 paste (T20/SP, Solaronix) using a doctor blade method (apparent surface area, 0.25 cm^2). Thickness of the layer (10 μm) was controlled by putting an adhesive tape (3*M*) on the FTO glass. After the casting, a sintering process was conducted in an oven at 550°C for 30 min with increasing heating rate of 3°C/min. Then, the TiO_2 electrodes at 80°C were soaked in a dye solution for 20 h under dark condition at room temperature. This dye solution consists of 0.3 m*M* of N719 (Solaronix) and anhydrous ethanol. The dye-coated electrode was rinsed with anhydrous ethanol and dried at room temperature. Similarly, a Pt-coated cathode electrode was prepared using a Pt sol (Pt-catalyst T/SP, Solaronix) by casting the sol on a cleaned FTO glass. The Pt electrode sol casted was sintered at 450°C for 30 min with increment rate of 3°C/min. The liquid electrolyte was comprised of 0.5*M* LiI, 0.05*M* I_2, 0.6*M* 1,2-dimethyl-3-propylimidazolium iodide (Solaronix), 0.5*M* 4-*tert*-butylpyridine (Aldrich) in 3-methoxypropionitrile (Aldrich).

To fabricate DSSCs, the substrate (1 cm × 1 cm) was sandwiched between the dye-adsorbed photo-anode and Pt-cathode electrodes. Both electrodes were fixed using two clips, and then the electrolyte solution was injected using a syringe between the two electrodes by a capillary force.

Characterization

A field emission-scanning electron microscopy (FE-SEM; S-4700, Hitachi) was used to observe surface morphologies of the porous substrates. Porosity values of the substrates were calculated from the following equation[12]:

$$\text{Porosity (vol \%)} = \left(1 - \frac{\rho_{ps}}{\rho_{polymer}}\right) \times 100 \quad (1)$$

where ρ_{ps} and $\rho_{polymer}$ are the densities of the porous substrate and polymer, respectively.

EIS was conducted using an IM6eX electrochemical workstation at an open circuit voltage with amplitude of 5 mV in the frequency range between 100 kHz and 0.01 Hz.[17] A cyclic voltammetry was conducted to obtain *J–V* curves and dark current densities using the electrochemical workstation at a scan rate of 20 mV/s. The photovoltaic property of a cell was measured under an illumination of 80 mW/cm^2 using a sulfur lamp source (at least more than three samples for each case). The FF was calculated from the following equation:

$$FF = \frac{P_{max}}{I_{SC}\, V_{OC}} \quad (2)$$

where P_{max} is the maximum electrical power density of the cell, I_{SC} the short-circuit current density, and V_{OC} the open-circuit voltage.

The conversion efficiency of the cell is calculated from the following equation:

$$\eta = \frac{P_{max}}{P_{in}} = \frac{I_{SC} \times V_{OC} \times FF}{P_{in}} \quad (3)$$

where P_{in} is the power input to the cell.

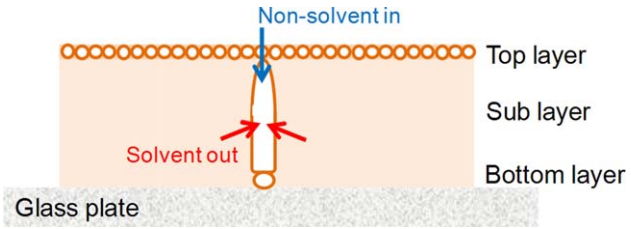

Figure 2. A schematic representation of a phase inversion process. [Color figure can be viewed in the online issue, which is available at wileyonlinelibrary.com.]

RESULTS AND DISCUSSION

There are several types of phase inversion methods[18]: thermally induced phase separation, air-casting of a polymer solution, immersion precipitation, and precipitation from the vapor phase. In the immersion precipitation method, pores are formed when the cast polymer is immersed in a nonsolvent such as deionized water. The organic solvent in the polymer film is rapidly extracted from the cast polymer because it is miscible with water. However, the polymer is immiscible in the nonsolvent, thus phase separation is occurred. As a result, there are two types of regions inside the cast polymer depending on polymer content, that is, polymer-rich and polymer-poor phases. The two polymer regions subsequently undergo to form polymer backbone structure and pores inside the cast substrate, respectively. A schematic of a phase inversion method is shown in Figure 2. At this step, the pore structures and diameters are determined according to the demixing kinetics of the solvent into the nonsolvent. In case of a method of precipitation from the vapor phase, humidifying procedure is additionally conducted before immersing the polymer into a nonsolvent compared to the immersion precipitation method. This vapor-induced phase inversion has been widely conducted to form sponge-type or comb-type porous substrates.[19]

Surface and cross-sectional morphologies of the PSs are shown in Figure 3. There are significant differences in structural shapes depending on the humidification process. When PSs were fabricated without humidification (PS-WOH), finger-type structures were observed with straight internal morphologies. It is noted that a top surface represents the layer which directly contacts the nonsolvent during the phase inversion process, whereas a bottom surface faces to the supporting glass (Figure 2). At the top surface [Figure 3(a,d)], in the magnified images, dense skin layers were formed, showing small pores in the range of 5–10 nm. At the bottom of the substrate, relatively bigger pores in the range of 0.2–0.5 μm were observed [Figure 3(c,f)]. In cases of PSs with the humidification process (PS-H), sponge-type structures were observed with droplet-shaped morphologies. At the top surface, bigger pores [Figure 3(g,j)] in the range of about 10–30 μm were observed than those in the range of about 2–5 μm at the bottom surface of the substrates [Figure3(i,l)].

The only difference is using the humidification process in the fabrication procedures of the PS-WOH and PS-H. In the former one, the cast polymer film was directly immersed in water as a nonsolvent without any humidification process. The NMP solvent in the polymer solution was rapidly extracted by mixing with water in the bath, resulting in very fast demixing kinetics of the polymer and NMP.[16] Thus, the hollow-like straight inner morphologies were formed, which is called a finger type structure. In addition, the fast kinetics of mixing between NMP and water is responsible for the dense skin layer with small pores at the top surface. At the bottom layer, however, relatively bigger pores were formed because of a slower kinetics of the phase inversion which propagates from the top surface to the bottom.

In case of the PS-H, the polymer film was maintained for several minutes in the container filled with a humidifying gas before immersing in the nonsolvent bath. This humidification process induces the slower mixing kinetics between the solvent in the cast polymer and the nonsolvent followed by the film is subsequently immersed in the bath for completion of the phase inversion. The slower kinetics is mainly owing to the lower activity of the vapor which penetrates through the polymer film. This low diffusion of the nonsolvent resulted in symmetry morphologies.

The use of BuOH as a cosolvent is known to affect a slower demixing kinetics owing to lower miscibility between the cosolvent of BuOH and the nonsolvent of water, forming larger pores.[20] In the case of PS-H of 1 : 4 : 1, larger pores at the bottom layer and clearer droplet-shaped polymer structures at the top layer were observed than those in the case of PS-H of 1 : 5 : 0. However, in cases of PS-WOH, no significant discrepancy was found regardless of cosolvent content except the inner tilted morphologies. Porosity values of the PS-H were 70.4 and 77.3% for the cases of 1 : 4 : 1 and 1 : 5 : 0, respectively, whereas those of PS-WOH were 74.5 and 83.0%, respectively.

Photocurrent–voltage characteristics of the quasi-solid-state electrolytes were examined according to the contacting top (top-TiO_2) and bottom (bottom-TiO_2) surfaces of substrates to the TiO_2 layer, respectively (Figure 4). As shown in Figures 5(a) and 6(a), in both cases, the cells with the quasi-solid-state electrolytes showed higher V_{OC} values between 0.71 and 0.75 V than that of 0.62 V with the liquid electrolyte. Higher V_{OC} values by about 0.1 V of the quasi-solid-state electrolytes are attributed to the Lewis basicity of the BPPO polymer.[12,15] The BPPO polymer contains functional groups of ether and bromine in the polymer structure, which are known to hard and soft bases, respectively, in solid-state electrochemistry.[21] It is explained that the BPPO polymer contacting on the TiO_2 layer shifted the flat band in TiO_2 at photo-anode to a negative range owing to the basicity of the polymer.[9] In addition, coordination of cations in electrolyte to the BPPO functional groups increased V_{OC}.[12,22] Lower cation concentration vicinity of the TiO_2 layer owing to the coordination suppresses recombination of I_3^- and electron trapping, thus increasing V_{OC}. Dark current density values demonstrate the higher V_{OC} values of the quasi-solid-state electrolytes for both top and bottom surfaces of the PSs as shown in Figures 5(b) and 6(b), respectively. Dark current represents the backward electron charge injection from TiO_2 layer into I_3^- in electrolytes and it implies electron losses by electrolytes.[23,24] Based on the dark current density at 0.6 V, the liquid electrolyte showed the highest value of 2.24 mA/cm^2. The quasi-solid-state electrolytes of PS-WOH varied between 0.28 and 0.45 mA/cm^2,

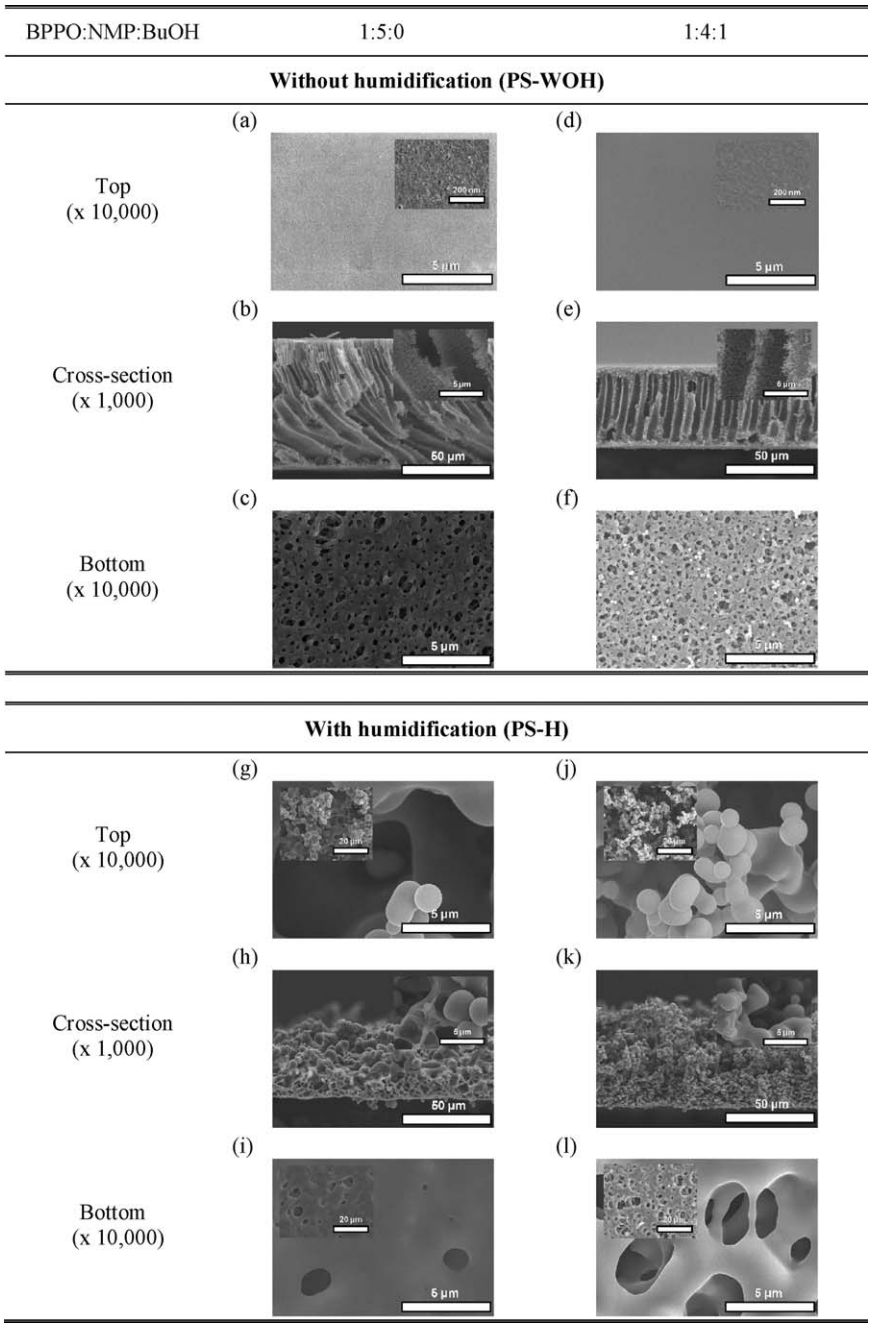

Figure 3. SEM images of the porous substrates prepared by the phase inversion method depending by varying the humidification condition and cosolvent composition.

whereas those of PS-H varied between 0.60 and 0.68 mA/cm^2 (Tables I and II). The dark current trend inversely coincides with the V_{OC} value trend in which the highest V_{OC} values of 0.74 and 0.75 V were obtained with the PS-WOH and the lowest value of 0.62 V with the liquid electrolyte. Large surface areas of the PS-WOH having small pores seem to maximize the coordination effects, resulting in higher V_{OC} [Figure 3(b,e)]. Additionally, smaller volume of the liquid electrolyte in quasi-solid-state electrolytes directly covering the TiO_2 layer reduces the total amount of I_3^-, thus, recombination and dark current would be further suppressed.[9]

Current density of the liquid electrolyte showed the highest current density of 9.06 mA/cm^2 and conversion efficiency of 4.65%. Among the PSs, the PS-H with the ratio of 1 : 4 : 1 showed higher current density of 7.20 and 7.66 mA/cm^2 and conversion efficiency of 3.60 and 3.86%, respectively, for the top and bottom surfaces (Tables I and II). Higher current densities of the PS-H are explained by the bigger pore sizes at both top and bottom surfaces as well as good interconnectivity of the tortuous pores inside the substrate.[19,25–27] The PS-WOH of 1 : 4 : 1 also exhibited comparable conversion efficiencies of 3.58 and 3.66% with current densities of 6.48 and 6.79 mA/cm^2.

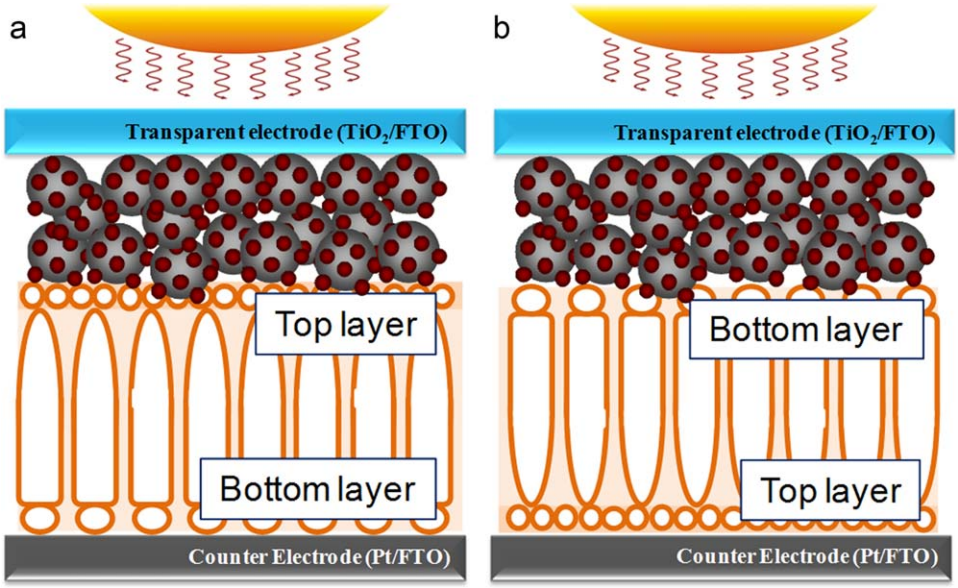

Figure 4. Schematic representations of DSSCs with the quasi-solid-state electrolytes according to the facing surface of the PS to the TiO_2 electrode: (a) a top layer of a PS contacts the TiO_2 layer (top-TiO_2) and (b) a bottom layer of a PS contacts the TiO_2 layer (bottom-TiO_2). [Color figure can be viewed in the online issue, which is available at wileyonlinelibrary.com.]

Although the straight finger-type structures of PS-WOH of 1 : 4 : 1 are advantageous for diffusion of iodide species than the tortuous structure, the dense layers with small pores at the top surfaces prohibited diffusion of triiodide through the quasi-solid-state electrolytes, resulting in the lower current densities and conversion efficiencies than the PS-H of 1 : 4 : 1.

However, the PS-H of 1 : 5 : 0 showed the lowest conversion efficiency of 1.10 and 0.98% although it has large pore structures at the top surface. The lower efficiencies are mainly owing to the lower current densities. It seems that the pores inside the PSs were not properly interconnected, prohibiting transport of iodide species. Thus, it is crucial to obtain both good interconnectivity of internal structures and proper pore sizes at the interface of PSs for better diffusion and photo-voltaic performance of a quasi-solid-state electrolyte. In all cases of the electrolytes, comparisons of the contacting surfaces of top and bottom the PS showed no significant discrepancy on the photo-voltaic efficiency.

Impedance spectra of the quasi-solid-state electrolytes were compared as shown in Figure 7. The theoretical impedance (Z) of an electrochemical system is composed of real and imaginary components. In case of a combination of a solution resistance (R_Ω) and a parallel of charge-transfer resistance (R_{ct}) and double-layer capacitance (C_d) according to the Randle equivalent circuit, the real (R_{RE}) and imaginary (R_{IM}) components are described as follows[28]:

$$Z_{RE} = R_\Omega + \frac{R_{ct} + \sigma\omega^{-1/2}}{(C_d\sigma\omega^{1/2}+1)^2 + \omega^2 C_d^2 (R_{ct} + \sigma\omega^{-1/2})^2} \quad (4)$$

$$Z_{IM} = \frac{\omega C_d (R_{ct} + \sigma\omega^{-1/2})^2 + \sigma\omega^{-1/2}(\omega^{1/2} C_d\sigma + 1)}{(C_d\sigma\omega^{1/2}+1)^2 + \omega^2 C_d^2 (R_{ct} + \sigma\omega^{-1/2})^2} \quad (5)$$

where $\omega = 2\pi f$ (f is the frequency).

At a low frequency range, as the $\omega \to 0$, the equations approach a limiting form, showing a Warburg impedance term:

$$Z = R_\Omega + R_{ct} + \sigma\omega^{-1/2} - j\left(\sigma\omega^{-1/2} + 2\sigma^2 C_d\right) \quad (6)$$

At a high frequency range, as the $\omega \to \infty$, the Warburg impedance becomes insignificant.

$$Z(\omega) = \left(R_\Omega + \frac{R_{ct}}{1+\omega^2 R_{ct}^2 C_d^2}\right) - j\left(\frac{\omega R_{ct}^2 C_d}{1+\omega^2 R_{ct}^2 C_d^2}\right) \quad (7)$$

$$Z(\omega) \cong \left(R_\Omega + \frac{1}{\omega^2 R_{ct} C_d^2}\right) - j\left(\frac{1}{\omega C_d}\right) \cong R_\Omega \quad (8)$$

The impedance spectra are interpreted with an equivalent circuit (Figure 8).[10,29,30] The intercept at the highest frequency is known as a series resistance (R_S) containing resistances of the electrolyte, conducting FTO glass, and electrical wires of the system. The first semi-circle at a high frequency range represents a charge-transfer resistance at the Pt/electrolyte interface (R_{Pt}). At an intermediate frequency range, the second semi-circle represents a charge-transfer resistance at the TiO_2/electrolyte interface (R_{TiO2}). The last one appearing at a low frequency is related with a diffusion limitation of the electrolyte (R_{Diff}). The results were fitted based on the equivalent circuit and the fitted results are summarized in Table III.

Based on the quasi-solid-state electrolytes in which the top layers of substrates are facing to the TiO_2 electrodes (top-TiO_2), the PS-WOH with 1 : 5 : 0 and 1 : 4 : 1 showed R_S of 9.7 and 9.6 Ω, R_{Pt} 30.4 and 26.2 Ω, and R_{TiO2} 51.1 and 44.7 Ω, respectively. Meanwhile, the PS-H with 1 : 5 : 0 and 1 : 4 : 1 showed slightly smaller R_S of 8.8 and 8.0 Ω, significantly increased R_{Pt} of 96.2 and 52.9 Ω, and smaller R_{TiO2} of 25.9 and 34.1 Ω, respectively. Higher R_S of the PS-WOH are explained by the dense layers with small pore diameters which increased the

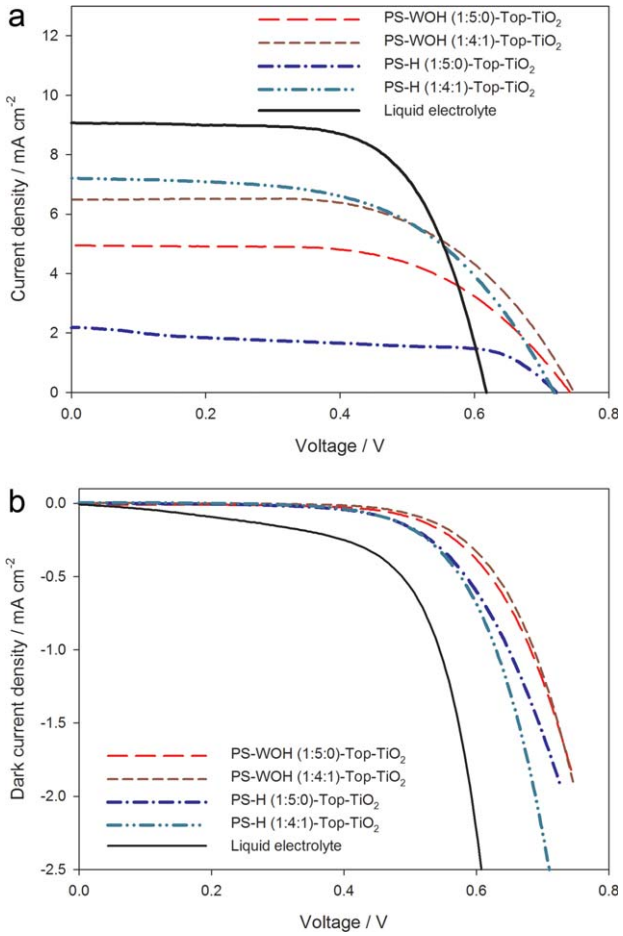

Figure 5. (a) Photocurrent–voltage curves and (b) dark current curves of DSSCs employing the liquid electrolyte and the quasi-solid-state electrolytes with the substrates. The top layers of the substrates are facing to the TiO_2 electrode (top-TiO_2). [Color figure can be viewed in the online issue, which is available at wileyonlinelibrary.com.]

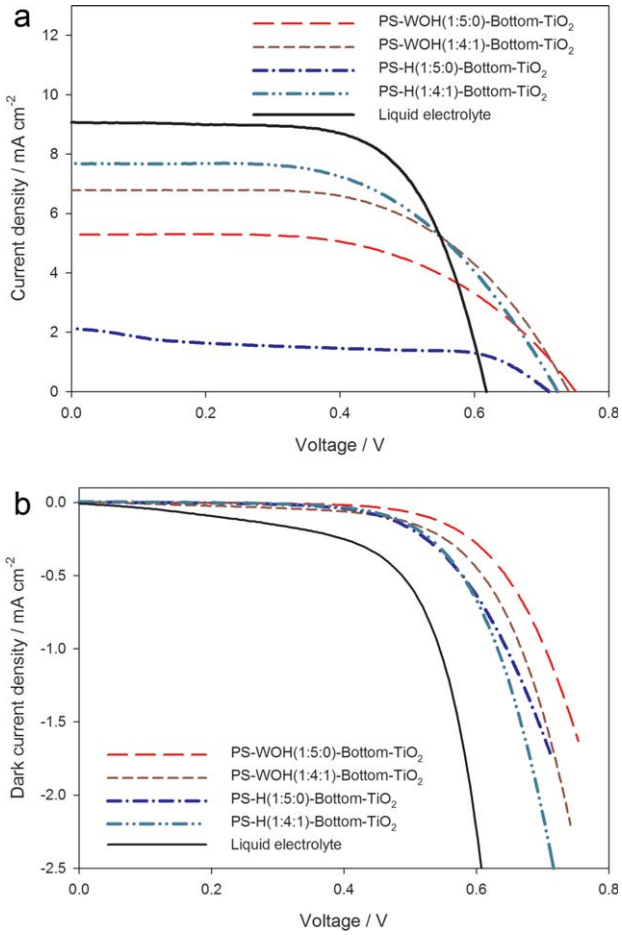

Figure 6. (a) Photocurrent–voltage curves and (b) dark current curves of DSSCs employing the liquid electrolyte and the quasi-solid-state electrolytes with the substrates. The bottom layers of the substrates are facing to the TiO_2 electrode (bottom-TiO_2). [Color figure can be viewed in the online issue, which is available at wileyonlinelibrary.com.]

overall electrolyte resistances at a high frequency range. The straight finger-type structures seem to be responsible for the smaller R_{Pt} owing to fast diffusion of I^-/I_3^- species through the quasi-solid-state electrolytes, affecting lower resistances for I_3^- reduction kinetics. Similarly, higher R_{Pt} of the PS-H are owing to the tortuous structures inside the substrates, prohibiting diffusion of I^- and I_3^- species by increasing the total length for transport. In contrast, the larger R_{TiO2} of PS-WOH than those of PS-H are owing to the fact that both substrates have dense layers at the interface of the TiO_2 layers. However, at this moment, it is not easy to clearly demonstrate the effects of the dense layer to the increased R_{TiO2}. It seems that diffusion of I^- and I_3^- vicinity of the TiO_2 layer is limited by the small pores at the intermediate frequency range, lowering dye-regeneration

Table I. Photovoltaic Properties of the Liquid Electrolyte and Quasi-Solid-State Electrolytes in Which the Top Layers of the PSs Are Facing to the TiO_2 Electrode (Top-TiO_2)

Type (top-TiO_2)	Without humidification (PS-WOH)		With humidification (PS-H)		Liquid electrolyte
Ratio (polymer : NMP : BuOH)	1 : 5 : 0	1 : 4 : 1	1 : 5 : 0	1 : 4 : 1	–
V_{OC} (V)	0.74	0.75	0.72	0.72	0.62
J_{SC} (mA/cm^2)	4.94	6.48	2.18	7.20	9.06
FF	0.59	0.59	0.56	0.56	0.67
Efficiency (%)	2.73	3.58	1.10	3.60	4.65
J_{dark} (mA/cm^2 at 0.6 V)	0.38	0.33	0.60	0.68	2.24

Table II. Photovoltaic Properties of the Liquid Electrolyte and Quasi-Solid-State Electrolytes in Which the Bottom Layers of the PSs are Facing to the TiO_2 Electrode (Bottom-TiO_2)

Type (bottom-TiO_2)	Without humidification (PS-WOH)		With humidification (PS-H)		Liquid electrolyte
Ratio (polymer : NMP : BuOH)	1 : 5 : 0	1 : 4 : 1	1 : 5 : 0	1 : 4 : 1	-
V_{OC} (V)	0.75	0.74	0.71	0.72	0.62
J_{SC} (mA/cm^2)	5.28	6.79	2.11	7.66	9.06
FF	0.56	0.58	0.52	0.56	0.67
Efficiency (%)	2.78	3.66	0.98	3.86	4.65
J_{dark} (mA/cm^2 at 0.6 V)	0.28	0.45	0.63	0.67	2.24

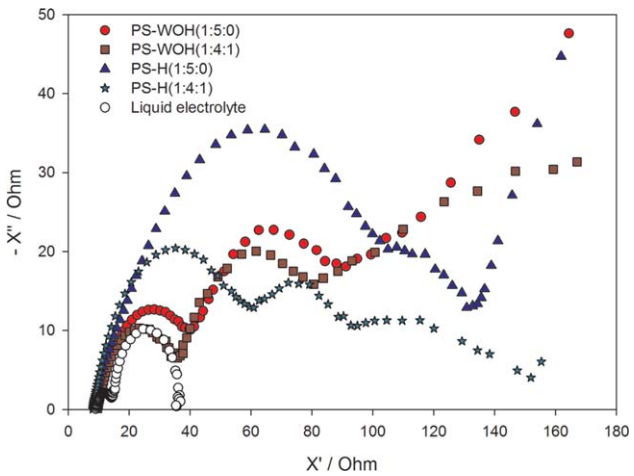

Figure 7. Impedance spectra of DSSCs using a liquid electrolyte and the quasi-solid-state electrolytes in which top layers of the porous substrates are facing to the TiO_2 electrodes. [Color figure can be viewed in the online issue, which is available at wileyonlinelibrary.com.]

and increasing the R_{TiO2}. In all cases except the PS-H of 1 : 4 : 1, Warburg resistances were observed at low frequency ranges. It means that diffusion of iodide species is retarded by the dense layers of PS-WOH and many closed pores in PS-H of 1 : 5 : 0. Although the PS-H of 1 : 5 : 0 seems to have a bigger pore size, the closed pores significantly prohibited the diffusion, thus, the electrolyte using the substrate obtained not only the highest R_{Pt} but also the lowest photocurrent density.

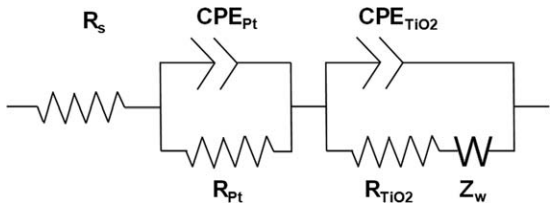

Figure 8. An equivalent circuit for the analyses of the impedance spectra of the DSSCs using the quasi-solid-state electrolytes and a liquid electrolyte.

The trends of impedance spectra of the top and bottom surfaces are compared in Figure 9. In all cases except the PS-H of 1 : 4 : 1, differences were mainly observed in R_{TiO2}, showing higher R_{TiO2} values of 76.7, 70.2, and 27.3 Ω, respectively, for the cases of bottom-TiO_2 than those of 51.1, 44.7, and 25.9 Ω, respectively, for the top-TiO_2. The resistance increased is explained by the properties of pores at the interface. As shown in Figure 10, Coster et al.[31] revealed the effects of a skin layer with smaller pore radii on resistive and capacitive characteristics in EIS; and ion exclusion in the pores. In cases of the bottom-TiO_2, the skin layer facing to the counter electrode seems to prohibit the reduction of I_3^- owing to the smaller pores with ion exclusion effects, further increasing the R_{TiO_2}.

CONCLUSIONS

Quasi-solid-state electrolytes were prepared using BPPO PSs prepared by a phase inversion method for DSSC applications. The SEM analyses confirmed variations of surface and cross-

Table III. Impedance Fitting Results of the Quasi-Solid-State Electrolytes with the Porous Substrates

Ratio		1 : 5 : 0				1 : 4 : 1		
		R_S	R_{Pt}	R_{TiO2}		R_S	R_{Pt}	R_{TiO2}
Without humidification (PS-WOH)	Top-TiO_2	9.7	30.4	51.1	Top-TiO_2	9.6	26.2	44.7
	Bottom-TiO_2	8.3	32.7	76.7	Bottom-TiO_2	11.2	26.6	70.2
		R_S	R_{Pt}	R_{TiO2}		R_S	R_{Pt}	R_{TiO2}
Humidification (PS-H)	Top-TiO_2	8.8	96.2	25.9	Top-TiO_2	8.0	52.9	34.1
	Bottom-TiO_2	7.5	118.7	27.3	Bottom-TiO_2	8.9	51.7	32.9

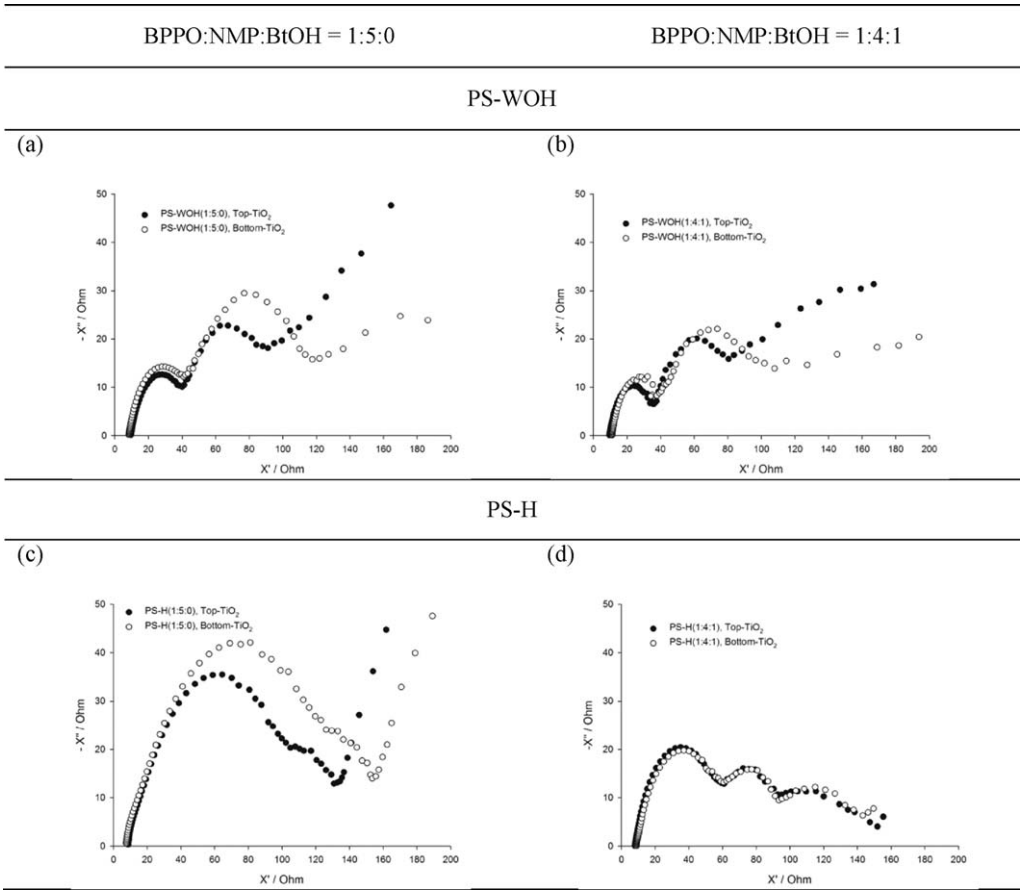

Figure 9. Impedance spectra of DSSCs with quasi-solid-state electrolytes with the porous substrates prepared by the phase inversion method.

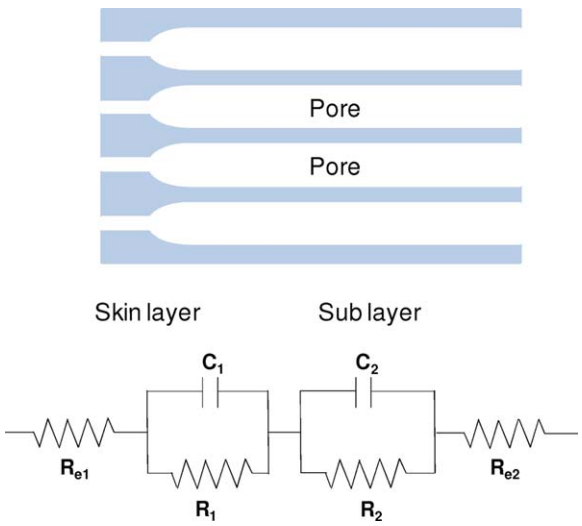

Figure 10. A schematic representation of a porous substrate in which skin and sublayers are formed (Ref. 31). An equivalent circuit for the membrane/electrolyte system consists of two parallel combinations of a resistance and capacitance for the skin (C_1 and R_1) and sub (C_2 and R_2) layers, and two interface electrolyte resistances (R_{e1} and R_{e2}). [Color figure can be viewed in the online issue, which is available at wileyonlinelibrary.com.]

sectional structures of the PSs according to the experimental conditions of humidification and cosolvent compositions. In all cases of the quasi-solid-state electrolytes, the increased V_{OC} values by about 0.1 V were observed compared to the conventional liquid electrolyte. The PSs prepared by the polymer solution of 1 : 4 : 1 (NMP : BPPO : BuOH) showed higher photocurrent densities and conversion efficiencies. Although the PS-H of 1 : 5 : 0 showed bigger pores at the surface, the inappropriately interconnected pore structures resulted in the lowest conversion efficiency. Thus, PSs for quasi-solid-state electrolytes require both large pore sizes and a good interconnectivity. The impedance results revealed that surface pore structures more dominantly affect the highest and intermediate frequency resistances of R_S and R_{TIO2}, respectively. Meanwhile, the straight inner structure is advantageous for the diffusion of I^-/I_3^- diffusion, showing lower R_{Pt}. Finally, the PS-H of 1 : 4 : 1 showed a lower diffusion limitation owing to the good interconnectivity than other substrates.

ACKNOWLEDGMENTS

This study was supported by the National Research Foundation of Korea Grant funded by the Korean Government. The BPPO provision by Prof. Tongwen Xu in USTC is also gratefully acknowledged.

REFERENCES

1. O'Regan, B.; Grätzel, M. *Nature* **1991**, *353*, 737.
2. Yella, A.; Lee, H.-W.; Tsao, H. N.; Yi, C.; Chandiran, A. K.; Nazeeruddin, M. K.; Diau, E. W.-G.; Yeh, C.-Y.; Zakeeruddin, S. M.; Grätzel, M. *Science* **2011**, *334*, 629.
3. Hinsch, A.; Veurman, W.; Brandt, H.; Aguirre, R. L.; Bialecka, K.; Jensen, K. F. *Prog Photovoltaics* **2012**, *20*, 698.
4. Cui, Y.; Zhang, J.; Wang, P.; Zhang, X.; Zheng, J.; Sun, Q.; Feng, J.; Zhu, Y. *Electrochim Acta* **2012**, *74*, 194.
5. Lim, S. J.; Kang, Y. S.; Kim, D.-W. *Electrochem. Commun.* **2010**, *12*, 1037.
6. Berginc, M.; Hočevar, M.; Krašovec, U. O.; Hinsch, A.; Sastrawan, R.; Topič, M. *Thin Solid Films* **2008**, *516*, 4645.
7. Kang, M.-S.; Kim, J. H.; Won, J.; Kang, Y. S. *J. Phys. Chem. C* **2007**, *111*, 5222.
8. Freitas, J. N. D.; Gonçalves, A. D. S.; Paoli, M.-A. D.; Durrant, J. R.; Nogueira, A. F. *Electrochim. Acta* **2008**, *53*, 7166.
9. Priya, A. R. S.; Subramania, A.; Jung, Y.-S.; Kim, K.-J. *Langmuir* **2008**, *24*, 9816.
10. Kim, J.-U.; Park, S.-H.; Choi, H.-J.; Lee, W.-K.; Lee, J.-K.; Kim, M.-R. *Sol. Energy Mater. Sol. Cells* **2009**, *93*, 803.
11. Park, S.-H.; Won, D.-H.; Choi, H.-J.; Hwang, W.-P.; Jang, S.-I.; Kim, J.-H.; Jeong, S.-H.; Kim, J.-U.; Lee, J.-K.; Kim, M.-R. *Sol. Energy Mater. Sol. Cells* **2011**, *95*, 296.
12. Seo, S.-J.; Yun, S.-H.; Woo, J.-J.; Park, D.-W.; Kang, M.-S.; Hinsch, A.; Moon, S.-H. *Electrochem. Commun.* **2011**, *13*, 1391.
13. Kim, D.-W.; Jeong, Y.-B.; Kim, S.-H.; Lee, D.-Y.; Song, J.-S. *J. Power Sources* **2005**, *149*, 112.
14. Zhang, J.; Han, H.; Xu, S.; Wu, S.; Zhou, C.; Yang, Y.; Zhao, X. *J. Appl. Polym. Sci.* **2008**, *109*, 1369.
15. Yang, H.; Ileperuma, O. A.; Shimomura, M.; Murakami, K. *Sol. Energy Mater. Sol. Cells* **2009**, *93*, 1083.
16. Witte, P. V. D.; Dijkstra, P. J.; Berg, J. W. A. V. D.; Feijen, J. *J. Membr. Sci.* **1996**, *117*, 1.
17. Park, H. C.; Kim, Y. P.; Kim, H. Y.; Kang, Y. S. *J. Membr. Sci.* **1999**, *156*, 169.
18. Woo, J.-J.; Seo, S.-J.; Yun, S.-H.; Xu, T.; Lee, J.; Moon, S.-H. *Electrochem. Commun.* **2010**, *12*, 148.
19. Wu, C.; Gong, Y.; Han, S.; Jin, T.; Chi, B.; Pu, J.; Jian, L. *Electrochim. Acta* **2012**, *71*, 33.
20. Taketani, Y.; Nagaoka, S.; Kawakami, H. *J. Appl. Polym. Sci.* **2004**, *92*, 3016.
21. Bruce, P. G. Solid State Electrochemistry; Cambridge University Press: New York, **2003**.
22. Kato, Y.; Ishihara, T.; Ikuta, H.; Uchimoto, Y.; Wakihara, M. *Angew. Chem. Int. Ed.* **2004**, *43*, 1966.
23. Barnes, P. R. F.; Anderson, A. Y.; Juozapavicius, M.; Liu, L. X.; Li, X. E.; Palomares, E.; Forneli, A.; O'Regan, B. C. *Phys. Chem. Chem. Phys.* **2011**, *13*, 3547.
24. Taura, H.; Daiguji, H. *Electrochim. Acta* **2010**, *55*, 3491.
25. Chmiola, J.; Yushin, G.; Gogotsi, Y.; Portet, C.; Simon, P.; Taberna, P. L. *Science* **2006**, *313*, 1760.
26. Seo, S.-J.; Jeon, H.; Lee, J. K.; Kim, G.-Y.; Park, D.; Nojima, H.; Lee, J.; Moon, S.-H. *Water Res.* **2010**, *44*, 2267.
27. Zhang, J.; Dow, N.; Duke, M.; Ostarcevic, E.; Li, J.-D.; Gray, S. *J. Membr. Sci.* **2010**, *349*, 295.
28. Bard, A. J.; Faulkner, L. R. Electrochemical Methods: Fundamentals and Applications, 2nd ed.; John Wiley & Sons: Hoboken, NJ, **2001**.
29. Wang, Q.; Moser, J.-E.; Grätzel, M. *J. Phys. Chem. B* **2005**, *109*, 14945.
30. Asano, T.; Kubo, T.; Nishikitani, Y. *J. Photochem. Photobiol. A Chem.* **2004**, *164*, 111.
31. Coster, H. G. L.; Kim, K. J.; Dahlan, K.; Smith, J. R.; Fell, C. J. D. *J. Membr. Sci.* **1992**, *66*, 19.